



pubs.acs.org/amrcda Article

Symmetry in Seeded Metal Nanocrystal Growth

Sara E. Skrabalak*



Cite This: Acc. Mater. Res. 2021, 2, 621-629

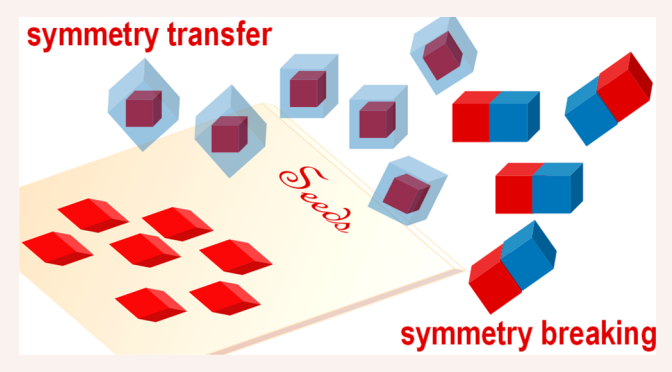


ACCESS

Metrics & More

Article Recommendations

CONSPECTUS: Symmetry underpins the structure and function of the world around us and is also captured in modern nanomaterials, where changing the symmetry of a nanocrystal or the interparticle spacing and orientation of nanocrystal building blocks in a superlattice can give new function. However, the synthesis and assembly of nanocrystals have been limited largely to simple compositions and structures. It remains a grand challenge to achieve nanocrystals with compositional and structural complexity while maintaining the monodispersity required for their use. This Account will illustrate through recent examples that seeded methods enable the synthesis of compositionally and structurally complex multimetallic crystals with defined and predictable symmetries for applications in plasmonics and catalysis. This outcome arises



because the barrier for heterogeneous nucleation (i.e., seeded) is lower than that of homogeneous nucleation, where seeds can serve as preferential sites for the growth of complex structures and crystal phases. Our analysis begins by considering metal overgrowth from single-crystalline seeds of different shapes and symmetries, where the kinetics of adatom addition to seeds relative to their diffusion across seeds accounts for the expressed nanocrystal shapes. These results are then compared to overgrowth from seeds with different internal structures (i.e., planar defects), where the relationships between nanocrystal size and volumetric strain energy and surface energy are discussed. A major finding from this analysis is that often the underlying symmetry of seeds can be predictably transferred to the final crystals during overgrowth processes. Consequences of this finding are the predictable syntheses of crystals with different hierarchies akin to snowcrystals as well as nanocrystals with complex compositions (e.g., quaternary nanoparticles). Yet, there are subtle aspects to seeded growth that pave a path toward examples where nanocrystal symmetry has been reduced compared to the original seeds in a controlled manner. As we found, both the concentrations of metal precursors and capping agents can impact whether symmetry is transferred or reduced during overgrowth. Examples from our laboratory will be placed in context to other reported strategies for symmetry breaking. As will be argued, understanding what conditions favor symmetry preservation versus symmetry reduction during seeded crystal growth is central to accessing next-generation crystal forms. The Account concludes by outlining synthetic challenges associated with forming nanoscale heterostructures with precise 3-D placement of different materials within a given nanocrystal as well as facet control within different material domain and interface engineering. We envision meeting these challenges through regioselective and chemoselective seeded syntheses for which a foundation is outlined herein.

■ INTRODUCTION

Nature exhibits its sense of symmetry in the beauty of a flower, the precision of a honeycomb, and the elaborate patterns of snowcrystals. Beyond the visual appeal of symmetrical forms, such structures can impart function. For example, orb spiders weave in a spiral pattern to maximize the strength of their webs, and bees construct honeycombs with close-packed hexagons to maximize honey storage. ^{1,2} Just as there are beautiful examples of how symmetry imparts function in the macroscopic world, the symmetries of modern nanomaterials and their assemblies are critical to their function. For example, polyhedral Ag nanocrystals have localized surface plasmon resonances that can be tuned by particle size and shape,³ and these nanocrystals can be assembled into superlattices where the degree of plasmon coupling between nanoparticle building blocks depends on their

orientation and spacing.⁴ However, the synthesis and assembly of nanomaterials have been limited to simple compositions and structures until recently.^{5–8}

Increasing the compositional and structural complexity of nanocrystals while maintaining high uniformity is a grand challenge that is being addressed with seeded methods. Seeded methods are a premier route to high-quality nanocrystal samples because structurally well-defined seeds can be selected and serve

Received: April 10, 2021 Revised: June 25, 2021 Published: July 17, 2021





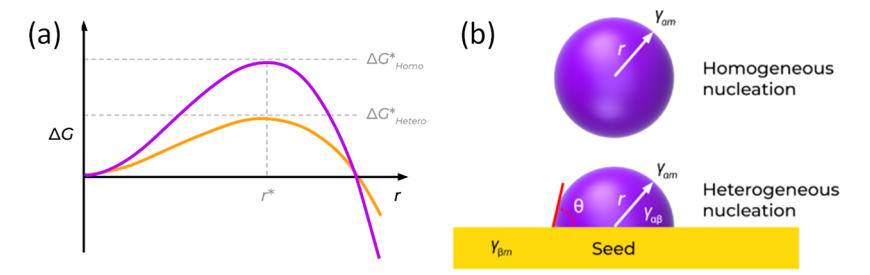


Figure 1. (a) Comparison of the change in Gibbs free energy as a function of particle radius for homogeneous and heterogeneous nucleation. ΔG^*_{Homo} and $\Delta G^*_{\text{Hetero}}$ are the barriers to homogeneous and heterogeneous nucleation, and r^* is the critical radius. (b) Depiction of homogeneous nucleation in solution and heterogeneous nucleation on a seed surface where r is the radius of the nucleus; θ is the contact angle between the nucleus and the seed surface; $\gamma_{\alpha m}$ is the increase in free energy per unit surface area of the nucleus; $\gamma_{\alpha \beta}$ is the nucleus-seed surface energy; and $\gamma_{\beta m}$ is seed-medium surface energy. Reproduced with permission from ref 14. Copyright 2020 American Chemical Society.

as preferential platforms for deposition of additional material, including completely new phases. $^{9-13}$ Such preferential deposition occurs when the barrier for heterogeneous (seeded) nucleation is lower than that of homogeneous nucleation (Figure 1a). In this analysis, three interfacial energy terms must be considered: γ_{am} for the nucleus-medium, $\gamma_{\beta m}$ for the substrate-medium, and $\gamma_{a\beta}$ for the nucleus-substrate (Figure 1b). This analysis indicates that the favorability of seeded processes will depend on the composition and faceting of the seeds and that of the depositing material.

Thus, homogeneous nucleation can occur in the presence of seeds when conditions do not favor surface wettability. Still, the judicious selection of seeds and reaction conditions offers many opportunities to synthesize nanocrystals of increasing compositional and structural complexity yet precision.

TRANSFER OF SYMMETRY IN SEEDED NANOCRYSTAL GROWTH

We do not have to look far to see the tendency for transfer of symmetry during seeded crystal growth. Consider, for example, the formation of snowcrystals. 15,16 As water in the atmosphere freezes, crystals in the shape of hexagonal prisms form on account of the preferred packing of water molecules. These crystals with D_{6h} symmetry then serve as preferential sites for water addition and crystallization. Even with the seemingly endless hierarchical snowcrystal forms, they largely preserve the D_{6h} symmetry of the hexagonal prisms in the earliest stages of crystal formation. The variability from one snowcrystal to the next arises from the different paths snowcrystals take through the atmosphere, each sampling different humidities, temperatures, and pressures. These changes in atmospheric conditions change the rate of water addition and are analogous to changes in supersaturation which are controlled through chemical means during nanocrystal nucleation and growth.

We have shown clearly the transfer of symmetry during seeded nanocrystal growth as part of our ongoing efforts to develop general routes to structurally defined multimetallic nanocrystals. For example, different shape-controlled AuPd alloy nanocrystals can be synthesized by coreducing Au and Pd salts with L-ascorbic acid (L-aa) in the presence of octahedral (O_h) Au seeds and cetyltrimethylammonium bromide (CTAB) as a capping agent. As shown by the scanning electron microscopy (SEM) images in Figure 2, these nanocrystals can adopt cubic, cubooctahedral, octahedral, and even 8-branched (concave) shapes; all have O_h symmetry like the initial seeds, reflective of transfer of symmetry. The different shapes arise from the changes in growth rates as a function of reaction

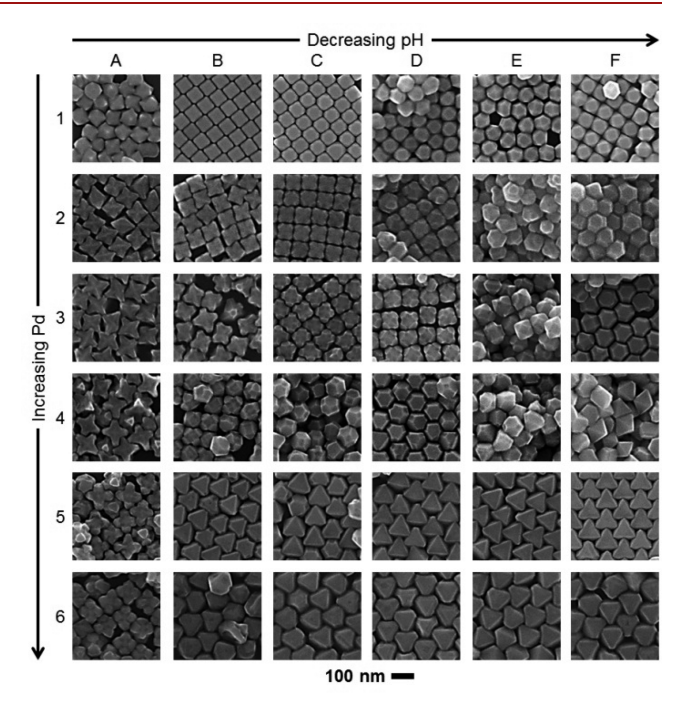


Figure 2. SEM images of Au–Pd nanocrystals with O_h symmetry prepared by seed-mediated coreduction from octahedral-shaped Au seeds. The nanocrystals reported in columns A–F were prepared with the addition of 2 mL of aqueous HCl solution to the Au seed solution prior to coreduction at concentrations of 0.0, 12.5, 25.0, 37.5, 50.0, and 62.5 mM, respectively. The values reported in Rows 1–6 were obtained with Au:Pd precursor ratios of 1:X where X is 0.01, 0.1, 0.2, 0.5, 1.0, and 2.0 during coreduction, respectively. Reproduced with permission from ref 19. Copyright 2012 American Chemical Society.

conditions, where fast adatom addition relative to adatom surface diffusion favors concave (kinetic) shapes and slow adatom addition relative to adatom surface diffusion favors convex (more thermodynamically favored) shapes. ²⁰ In this system, pH modulates the rates of precursor reduction, but other synthetic parameters also have been shown to serve as kinetic levers (e.g., overall precursor concentration and temperature) to access a variety of different crystal shapes during seeded overgrowth with transfer of symmetry. ¹¹

Given the straightforward connection between seed symmetry and final nanocrystal symmetry reflected in Figure 2, we also selected seeds of different shape and used them again for the synthesis of AuPd nanocrystals at conditions which favor branching (rate of metal deposition > rate of metal adatom diffusion). For example, Pd cubes (O_h) , Pd bars (D_{4h}) , Pd

octahedra (O_h) , and Pd tetrahedra (T_d) were used as seeds, each producing branched AuPd nanocrystals after seed-mediated coreduction (Figure 3). Products include 8-branched AuPd

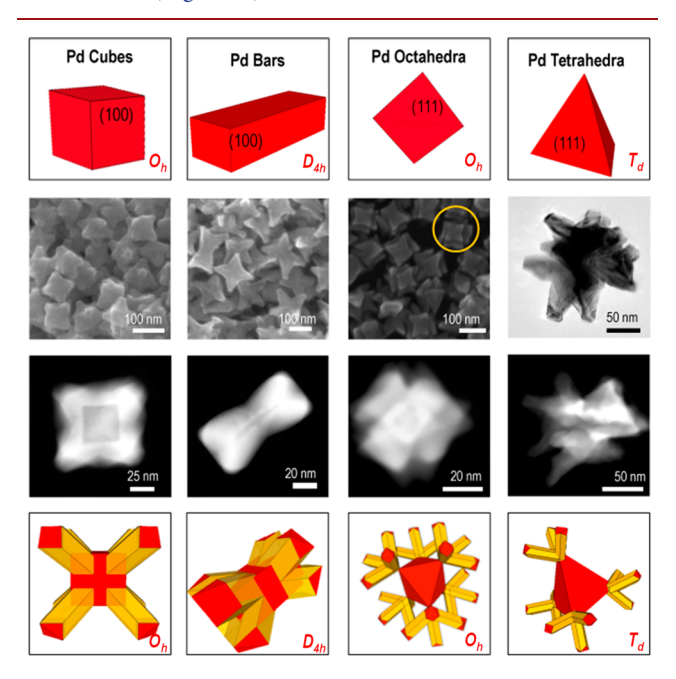


Figure 3. From left to right: AuPd nanocrystals with different symmetries prepared by seed-mediated coreduction from single-crystalline Pd nanocubes, Pd nanobars, Pd octahedra, and Pd tetrahedra. From top to bottom: structural model of the Pd seeds and their point group symmetries, SEM images of nanocrystal products (TEM image in the case of tetrahedral Pd seeds), STEM images of nanocrystal products, and structural models of nanocrystal products with their point group symmetries. The products include 8-branched AuPd nanocrystals with O_h symmetry, 8-branched AuPd nanocrystals with O_h symmetry, and 12-branched nanocrystals with T_d symmetry. Adapted with permission from ref 21. Copyright 2013 American Chemical Society.

nanocrystals with O_h symmetry from the Pd cubes, 8-branched AuPd nanocrystals with D_{4h} symmetry from the Pd bars, 24-branched AuPd nanocrystals with O_h symmetry from the Pd octahedra, and 12-branched AuPd nanocrystals with T_d symmetry from the Pd tetrahedra. The final nanocrystals all have the same symmetry of their initial seeds. Branches initiate at the vertices of the shape-controlled Pd seeds, and all proceed in $\langle 111 \rangle$ directions, accounting for the differences in number and also providing general design criteria for branched nanocrystals with defined symmetries.

All of the seeds discussed thus far are single-crystalline. A similar study was undertaken with shape-controlled Au seeds that contain 2-D planar defects (twins and stacking faults), again showing transfer of symmetry from AuPd overgrowth achieved by seed-mediated coreduction (Figure 4).²² That is, from Au decahedra (D_{5h}) , Au pentatwinned rods (D_{5h}) , Au icosahedra (I_h) , and Au nanoplates (D_{3h}) , branched nanocrystals were produced. Products include 10-branched AuPd rods with D_{5h} symmetry from both the Au decahedra and pentatwinned rod seeds, 20-branched AuPd nanocrystals with I_h symmetry from Au icosahedra, and pentapod-like AuPd nanocrystals with D_{3h} symmetry from Au nanoplates.

Although branched nanocrystals were produced like in the previous study, rather than branches emerging from the vertices of the seeds, they grow perpendicular from the {111}-

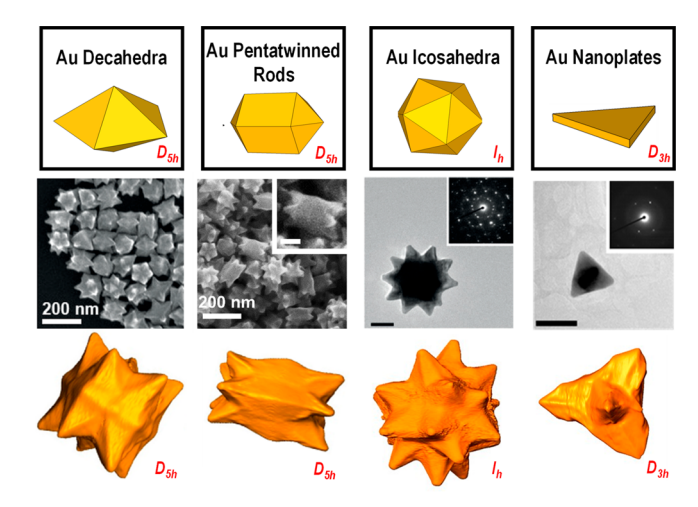


Figure 4. From left to right: AuPd nanocrystals with different symmetries prepared by seed-mediated coreduction from seeds with planar defects: Au decahedra, Au pentatwinned rods, Au icosahedra, and triangular Au nanoplates. From top to bottom: structural model of the Au seeds, SEM images of nanocrystal products (TEM images in the case of Au icosahedral and planar seeds; insets electron diffraction), and tomographic reconstructions of individual nanocrystals. The products include 10-branched AuPd nanocrystals with D_{5h} symmetry, longer 10-branched AuPd nanocrystals with I_h symmetry, and 5-branched AuPd nanocrystals with D_{3h} symmetry. Adapted with permission from ref 22. Copyright 2020 Wiley-VCH Publishing.

terminated faces of the seeds, with one branch per facet. To understand this observation, the total free energy of the crystal, G(T), must be considered. In a study of elastic strain energy effects in metal nanocrystals by Marks and Olvera de la Cruz, G(T) for multiply twinned crystals was approximated as

$$G(T) \approx V(W_{\rm V}^{\rm D} + \Delta \overline{G}_{\rm f}) + \sum_{i} A_{i} (\gamma_{i} + W_{\rm S}_{i}) + \gamma_{t} A_{t}$$
 (1)

where V is the NC volume; W_V^D is the per-volume strain energy; $\Delta \overline{G}_f$ is the change in free energy per unit volume; A is the surface area; W_S is the surface strain energy; and γ is the surface energy. The subscripts i and t refer to certain facets and the twin boundary, respectively. Their finite element analysis revealed that different decahedral shapes arise at different particle sizes from the balance between surface energy and volumetric strain energy. That is, convex decahedra are favored at small particle sizes, as this corresponds to when W_V^D is small and the free energy is dominated by the surface energy term. In contrast, star (concave) shapes are favored at larger particle sizes as W_V^D increases as a function of volume.

Considering this analysis in the context of our synthetic system, the volumetric strain energy should dominate over surface energy at some critical particle size, at which point the energy penalty for branch formation would be lower than that for increasing the twin plane dimensions. To assess this possibility, we quenched the reaction of AuPd deposition on decahedral Au seeds at different stages of overgrowth and analyzed the particles by microscopy.²² In the earliest stages, an increase in decahedral seed size was found without branching, corresponding to an increase in the twin dimensions. Longer reaction times only increased decahedral dimensions slightly, while branching became evident. These observations support the exchange between surface energy and volumetric strain energy. The simulations by Marks and Olvera de la Cruz also

found that the surfaces of the decahedra display the highest stress and strain energy densities at the face centers of the tetrahedral units and the center of the outer edges. This finding provides a possible explanation for why the branches emerge from face centers rather than vertices (as observed in the case of single-crystalline seeds), as metal deposition will be favored at high-energy sites under kinetically controlled growth conditions.

■ SUBTLE EFFECTS DURING TRANSFER OF SYMMETRY IN SEEDED NANOCRYSTAL GROWTH

One may note that growth from Au and Pd octahedra produces nanocrystals with different numbers of branches (Figure 2 versus Figure 3; 8- versus 24-branches) even though the chemistries producing these structures are the same and the symmetries of the resulting nanocrystals are the same, O_h . ^{19,21} This difference arises because the rate of adatom diffusion on seeds will vary as a function of seed composition. Our kinetic analysis found that Au deposits more rapidly than Pd. 25,26 Considering predominately Au adatoms on Au and Pd surfaces during the early stages of overgrowth, self-diffusion will be faster and makes Au seeds more susceptible to the adoption of intermediate shapes prior to branch growth. This possibility was verified by quenching at different times the reaction in which Au and Pd were depositing on Au octahedra. 25 As we found, nanocubes form as intermediate structures prior to branching, which ultimately emerge from the 8 vertices of the nanocubes to give 8-branched nanocrystals. This structure is the same as obtained from AuPd overgrowth from Pd nanocubes (Figure 3).

A second interesting observation comes from the use of Pd right bipyramids, which contain single twin planes, as seeds. Codeposition of Au and Pd yields 5-branched pentapods with D_{3h} symmetry (Figure 5).²¹ Two branches proceed from the axial vertices in (111) directions, while 3 branches proceed from the equatorial vertices in (112) directions, with the twin plane expanding through the 3 equatorial branches. This observation is in contrast to our study of Au nanocrystal seeds containing planar defects, where branches always extended from faces rather than vertices and did not contain planar defects (Figure 4).²² Analogous Au right bipyramids have not been studied as seeds, as a facile synthesis to this shape has yet to be developed for Au, but the distinct overgrowth behavior from Pd right bipyramids suggests that the energetics of twin formation varies with composition and could influence branch formation and direction. Additional studies are required.

A third interesting observation comes from the study of overgrowth from the Au seeds with planar defects.²² The "Transfer of Symmetry" section outlined the relationship between seed symmetry and final nanocrystal symmetry after overgrowth. However, symmetry preservation was not always achieved. Breaking of symmetry was particularly evident in the case of Au icosahedra as seeds, where branches grew perpendicular to the {111} facets. Often, we observed that not all of the facets would produce a branch. Au icosahedral seeds have 20 {111} facets, but our analysis of the resulting nanocrystals found the number of branches to vary between 10 and 20. Tomography analysis of the icosahedral Au seeds suggests this variation may arise from the imperfections in the seeds, where not all {111} facets were of equal surface area. In reality, the seeds are only quasi- I_h , where their imperfections are being transferred to the final nanocrystals. Our use of point group notation for different nanocrystal types reflects the idealized structure without consideration of defects or composi-

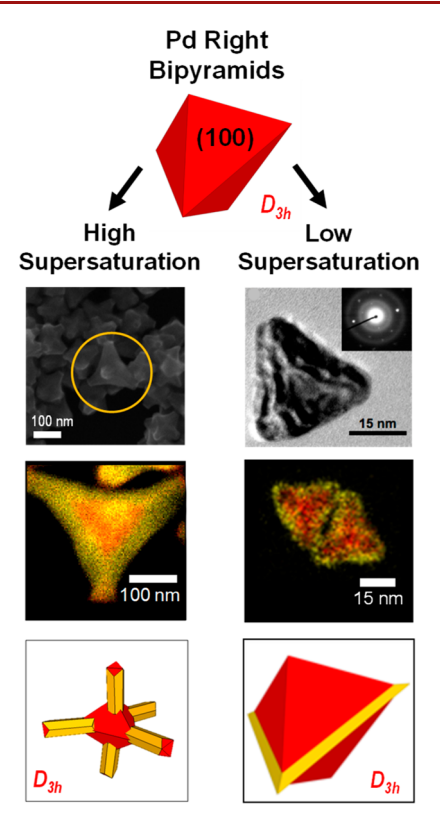


Figure 5. AuPd nanocrystals grown from singly twinned Pd right bipyramids under (left) high and (right) low supersaturation. (Left) From top to bottom, SEM image, STEM-EDS elemental mapping, and structural model of 5-branched AuPd nanocrystals. (Right) From top to bottom, TEM image (inset electron diffraction), STEM-EDS elemental mapping, and structural model of edge-decorated right bipyramids. In both elemental maps, yellow corresponds to Au, and red corresponds to Pd. Adapted with permission from refs 21 and 27. Copyright 2013 and 2017 American Chemical Society.

tional variations. This analysis also hints at a strategy by which symmetry breaking during seeded growth may be achieved by making use of the inherent imperfections of nanocrystal seeds, with greater discussion of this topic in the "Symmetry Reduction" section.

SEEDED CRYSTAL GROWTH TOWARD HIERARCHICAL STRUCTURES

The discussion in the "Transfer of Symmetry" section shows clearly how symmetry is transferred during seeded growth but also how different shapes of the same symmetry (e.g., a cube and octahedron) are possible through kinetic control during seeded growth. This realization inspired us to apply seeded growth sequentially to build up hierarchical structures, where the overall symmetry is governed by the initial seed, but the kinetics of the overgrowth process can be modulated to switch between different overgrowth motifs much in the manner that snowcrystals can adopt different forms. ^{28,29} The overall concept is outlined in Figure 6, where, for example, 8-branched AuPd nanocrystals with O_h symmetry can be used as seeds themselves for additional metal deposition from Au and Pd salts reduced with L-aa in the presence of CTAB.

Based on our analysis of overgrowth from single-crystalline seeds (Figure 3),²¹ we hypothesized that metal deposition would occur preferentially at the branch tips under kinetically controlled growth conditions. Yet, even with such regioselective

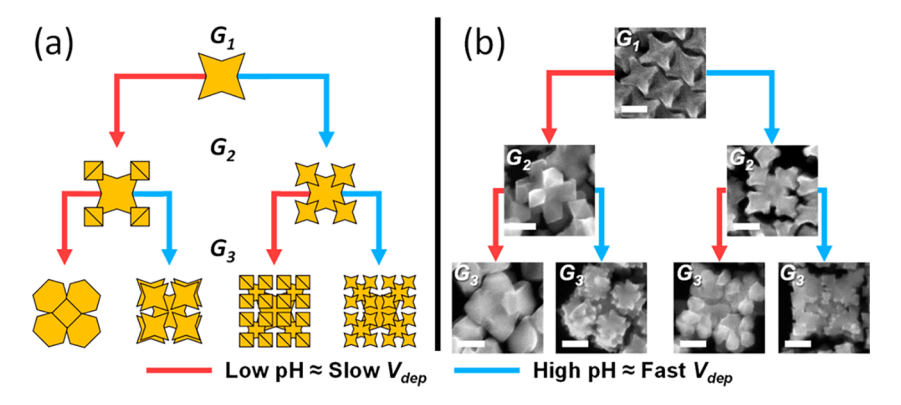


Figure 6. (a) Scheme depicting how nanocrystals with different hierarchies can be achieved by sequential seeded growth, denoted as generations G_1 through G_3 , where the red path denotes conditions where the rate of metal deposition ($V_{\rm dep}$) is slow relative to surface diffusion and the blue path denotes conditions where $V_{\rm dep}$ is fast relative to surface diffusion. (b) SEM images of Au–Pd nanocrystals achieved by the synthetic strategy depicted in (a) and based on coreduction of Au and Pd precursors with L-aa in an aqueous solution of CTAB at different reaction pHs. Adapted with permission from ref 29. Copyright 2020 American Chemical Society.

deposition, the form of the deposition can be controlled by the rate of metal deposition, as illustrated in Figure 2, as a function of reaction pH. Indeed, as shown in Figure 6, metal deposition occurs preferentially at the tips of the 8 branches, with the form of the metal deposition adopting octahedra at low pH (slow deposition rate) and multiple branches all proceeding in $\langle 111 \rangle$ directions at higher pH (fast deposition rate). These new nanocrystals can then serve as second-generation " G_2 " seeds for an additional round of overgrowth, with even more hierarchical structures being accessed (Figure 6). We anticipate the principles of kinetically controlled sequential seeded growth to be general to other material systems, opening up pathways to achieve structurally complex crystal with precision.

INCREASING COMPOSITIONAL COMPLEXITY DURING SEEDED CRYSTAL GROWTH

Thus far, the examples discussed all use similar chemistry: coreduction of Au and Pd salts with L-aa in the presence of Au or Pd seeds and the aqueous CTAB system. The resulting AuPd nanocrystals display interesting plasmonic and photothermal properties on account of their shape and composition, ^{30–33} but other compositions are desirable for different applications. For example, Pt-based alloys are attractive for catalysis. ¹⁴ In this regard, the aqueous CTAB system is limiting as only a handful of metal salts can be reduced at similar rates with L-aa in the same pH window, and many metals are too susceptible to oxidation after nanoparticle formation under these conditions. ^{34,35} Thus, we sought to demonstrate the versatility of seed-mediated coreduction in oleylamine-based systems, another common reaction medium for metal nanoparticles. ³⁶

In particular, we were interested in depositing PtM (where M = Cu, Ni, Fe, and Co) shells on intermetallic nanoparticle seeds to create core@shell nanoparticles for electrocatalytic applications given the promise of PtM nanoparticles for the oxygen reduction reaction, along with other processes.³⁷ The intermetallic cores were selected to impart durability to the alloy shells, i.e., stabilize the shell metals against oxidation and dissolution, by ordering the atoms at the core@shell interface to enhance the binding between the core and shell materials.³⁸ The alloy shells were also strained by the lattice mismatch between the core and shell materials to modify catalytic performance.^{38–40} We recently reviewed this work,⁴¹ but as we would like to emphasize here, the quasi-spherical morphology of the

intermetallic seeds was transferred to the final nanoparticles with random alloy surfaces. Shown in Figure 7 is characterization of core@shell intermetallic PdCu@PtCu random alloy nanoparticles prepared by coreducing platinum bromide (PtBr₂) and copper acetylacetonate (Cu(acac)₂) under an inert atmosphere with 1,2-hexadecanediol in a heated mixture of oleylamine, 1-octadecene, and PdCu seeds, illustrating this point. 40 The composition of the shell surface could be tuned

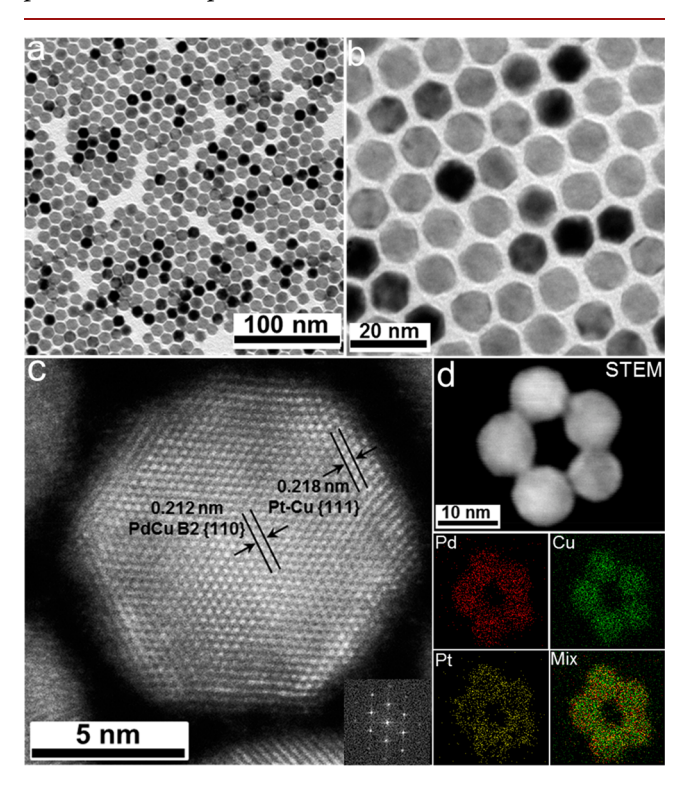


Figure 7. TEM images at (a) low and (b) high magnification of core@ shell PdCu@PtCu nanoparticles consisting of intermetallic cores and random alloy shells. (c) Spherical aberration (C_s)-corrected STEM image of an individual nanoparticle showing the coherent interface between the core and shell compositions. (d) STEM image of five core@shell PdCu@PtCu nanoparticles and corresponding elemental mapping by STEM-EDS, where red corresponds to Pd, green corresponds to Cu, and yellow corresponds to Pt. Reproduced with permission from ref 40. Copyright 2017 American Chemical Society.

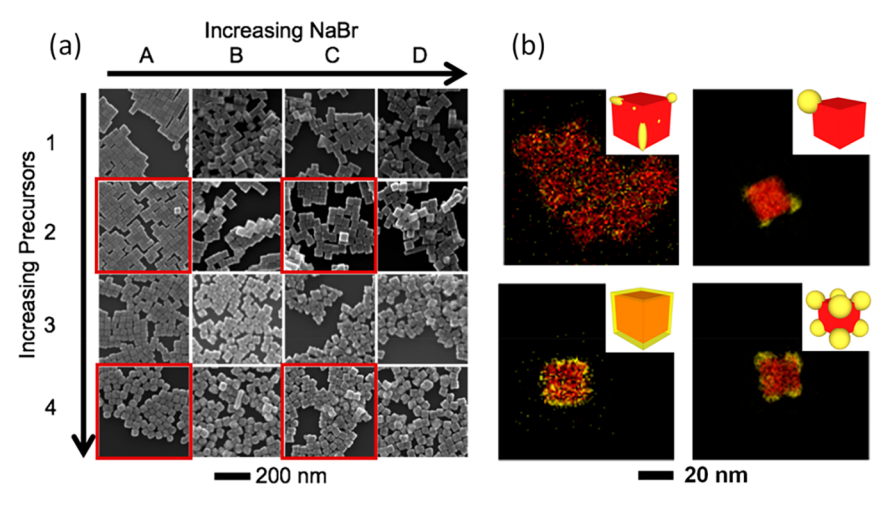


Figure 8. (a) SEM images of Au–Pd nanocrystals produced as a function of precursor concentration (where 1–4 corresponds to 10 μ L, 25 μ L, 50 μ L, and 100 μ L, respectively, of 10 μ M H₂PdCl₄ and 1 mM HAuCl₄) and bromide concentration (where A–D corresponds to 400 μ mol of CTAB, 200 μ mol of CTAB and 200 μ mol of NaBr, 200 μ mol of NaBr, and 200 μ mol of CTAB and 600 μ mol of NaBr, respectively). (b) STEM-EDS elemental mapping of Au–Pd nanocrystals shown in 2A, 2C, 4A, and 4C; red indicates Pd and yellow indicates Au. Adapted with permission from ref 27. Copyright 2017 American Chemical Society.²⁷

readily by changing the precursor identity and ratio for optimized catalytic performance.³⁹

We also anticipate that shape-controlled nanoparticles (e.g., nanocubes, octahedra, etc.) with this level of compositional versatility and complexity can be accessed by seed-mediated coreduction, where the shape and initial symmetry of the seeds can be transferred to the final nanocrystals. This assertion is based on our report of intermetallic PdCu@PtCu random alloy nanocubes in the previously described oleylamine-based system; however, such shape control was achieved by judicious addition of capping agents (triphenylphosphine) during the seedmediated coreduction process not the selection of shapecontrolled seeds. 42 We note that there are fewer reports of highquality shape-controlled metal nanoparticles prepared in this or closely related solvent systems, necessitating that seeds prepared in aqueous media be transferred into the organic phase to test this hypothesis. 43,44 Fewer reports of shape-controlled metal nanoparticles in this system compared to others likely has to do with the combination of capping agents used and high reaction temperatures (200–300 $^{\circ}$ C). That is, the capping agents commonly employed may be less discerning between different crystal facets than those used in water, while the high reaction temperatures promote adatom diffusion and more thermodynamically favored crystal shapes. Thus, while tuning between cubic and octahedral shapes is likely feasible, particularly when templated by shape-controlled seeds, access to a suite of kinetic structures (e.g., concave nanoparticles) across a diversity of compositions will require synthetic innovations to limit rapid adatom diffusion.

SYMMETRY REDUCTION IN SEEDED NANOCRYSTAL GROWTH

A central theme of this *Account* is the ability to achieve high-quality nanocrystals with compositional and structural complexity on account of transfer of symmetry during seeded growth. A useful development would be the ability to start with high-symmetry seeds and reduce nanoparticle symmetry during overgrowth in a controlled manner. This ability would provide new properties on account of the novel shapes that could be accessed. This ability has been studied by a number

of groups. For example, Xia and co-workers reported dimeric Ag–Pd nanobars and nonconcentric core@shell Ag–Pd nanocubes when the rate of Ag adatom deposition on Pd nanocubes was slow. The nanobars mark a break in symmetry from the seeds with O_h symmetry, while the nonconcentric core@shell Ag–Pd nanocubes do once composition is considered. As they explained, the concentration of Ag growth species was too low to achieve nucleation on all faces of the nanocubes, leading to nucleation of only one Ag island per seed at low supersaturation and three islands per seed at moderate supersaturation.

We also found that controlled symmetry reduction was possible in seeded overgrowth. Like the work by Xia and coworkers, supersaturation played a critical role, but we also systematically studied the effect of capping agents in symmetry reduction. In our study, Pd nanocubes were used as seeds for deposition of Au-rich AuPd domains, where HAuCl₄ and H₂PdCl₄ were coreduced at 25 °C using L-aa in the aqueous CTAB system to which additional bromide was added.²⁷ The effect of metal precursor concentration and bromide concentration was studied, where bromide is a capping agent for {100} facets in this system. Microscopy characterization of the products shown in Figure 8 reveals that only a few vertices per cubic seed support metal deposition at low supersaturation, and the number of vertices with metal deposition increases with supersaturation. This regioselective deposition, however, was only strongly evident with a high concentration of bromide, which blocked deposition from the seed faces. Differences in capping may account (at least in part) for why deposition may occur preferentially on seed vertices in one system and seed faces in another, but additional experiments are required.

CONCLUSIONS AND OUTLOOK

Seeded methods are a premier pathway to metal nanocrystals with compositional and structural complexity, providing a preferential platform for the deposition and growth of new phases with size and shape control and even with some degree of regioselectivity. Much of the utility stems from predictable transfer of symmetry during seeded overgrowth and the ability to control the expressed shape through known kinetic levers. We

used our research with metal nanocrystals to illustrate these points, but the same concepts are evident, if not as systematically studied, for other material classes. Still, we are far from realizing the "Materials by Design" framework for nanoscale materials even within the context of seeded methods.⁵⁰ To achieve this vision, additional research into controlled symmetry reduction and heterostructure formation is needed.

Considering symmetry reduction during seeded overgrowth, the intrinsic heterogeneity of nanoparticle seeds likely contributes to the observed regioselectivity at low supersaturation. Considering nanocubic seeds as an example, the vertices of these seeds are not atomically precise even in the most monodisperse samples and display different degrees of curvature. 51 These differences between vertices give different barriers to metal deposition. 14 Still, these different barriers to metal deposition are likely quite small, so methods that could amplify the differences may be useful. With this point in mind, exploiting crystallographically different features of seeds may offer more opportunities. For example, right bipyramidal seeds have crystallographically inequivalent vertices (axial versus equatorial, the latter of which contains the twin plane). The barriers to deposition at these inequivalent vertices will be different. As we found, this difference led to metal deposition preferentially at only equatorial positions at low supersaturation (Figure 5).²⁷ However, this regioselective deposition was not accompanied by a change in overall particle symmetry, but selection of appropriate seeds with crystallographically inequivalent features coupled with selective deposition conditions and capping agents could achieve this objective.

As the roles of seed symmetry and deposition kinetics in determining the final nanocrystal shape hold across material classes, the prospects of precisely integrating different types of materials into one nanocrystal heterostructure are high. There are already eloquent examples of metal-semiconductor heterostructures of various forms, for example. 52,53 Now, frontiers in seeded growth include facet control within different material domains, interface engineering, and 3-D placement of different materials within a given nanocrystal. Such new multicomponent nanocrystals could then serve as templates in chemoselective transformations (e.g., ion exchange and galvanic replacement) to increase chemical complexity. 5,54,55 Establishing general routes to achieve these various objectives would truly establish seeded methods as a predictable route to novel nanomaterials, where shape-controlled seeds provide a versatile platform for symmetry-guided overgrowth.

AUTHOR INFORMATION

Corresponding Author

Sara E. Skrabalak — Department of Chemistry, Indiana University — Bloomington, Bloomington, Indiana 47405, United States; orcid.org/0000-0002-1873-100X; Email: sskrabal@indiana.edu

Complete contact information is available at: https://pubs.acs.org/10.1021/accountsmr.1c00077

Author Contributions

This manuscript was written solely by S.E.S.

Funding

This work was supported by U.S. NSF CHE #1904499 and U.S. DOE BES Award DE-SC0018961.

Notes

The author declares no competing financial interest.

Article

Biography

Sara Skrabalak received her B.A. in chemistry from Washington University in St. Louis in 2002 where she conducted research with Professor William Buhro. She then moved to the University of Illinois at Urbana—Champaign, completing her Ph.D. in chemistry in the fall of 2006 with the tutelage of Professor Kenneth Suslick. After postdoctoral research at the University of Washington-Seattle with Professors Younan Xia and Xingde Li, she began her independent career in the Chemistry Department at Indiana University—Bloomington in 2008, where she was named the James H. Rudy Professor in 2015. She is a recipient of many accolades, most recently being named a fellow of the American Association for the Advancement of Science in 2020. Professor Skrabalak is Editor-in-Chief for both Chemistry of Materials and ACS Materials Letters. Her research group focuses on nanomaterial design and synthesis for applications in catalysis, solar energy use, secured electronics, chemical sensing, and more (https://skrablab. sitehost.iu.edu/).

ACKNOWLEDGMENTS

S.E.S. would like to thank all of the current and former group members who made this work possible as well as our collaborators who have provided such incredible insight into our materials.

REFERENCES

- (1) Griffiths, J. R.; Salanitri, V. R. The Strength of Spider Silk. *J. Mater. Sci.* **1980**, *15*, 491–496.
- (2) Chamberland, M. Single Digits: In Praise of Small Numbers; Princeton University Press: NJ, 2015; p 241.
- (3) Cobley, C. M.; Skrabalak, S. E.; Campbell, D. J.; Xia, Y. Shape-Controlled Synthesis of Silver Nanoparticles for Plasmonic and Sensing Applications. *Plasmonics* **2009**, *4*, 171–179.
- (4) Tao, A.; Sinsermsuksakul, P.; Yang, P. Tunable Plasmonic Lattices of Silver Nanocrystals. *Nat. Nanotechnol.* **2007**, *2*, 435–440.
- (5) Steimle, B. C.; Fenton, J. L.; Schaak, R. E. Rational Construction of a Scalable Heterostructured Nanorod Megalibrary. *Science* **2020**, 367, 418–424
- (6) Chen, P.-C.; Liu, X.; Hedrick, J. L.; Xie, Z.; Wang, S.; Lin, Q.-Y.; Hersam, M. C.; Dravid, V. P.; Mirkin, C. A. Polyelemental Nanoparticle Libraries. *Science* **2016**, 352, 1565–1569.
- (7) Paik, T.; Murray, C. B. Shape-Directed Binary Assembly of Anisotropic Nanoplates: A Nanocrystal Puzzle with Shape-Complementary Building Blocks. *Nano Lett.* **2013**, *13*, 2952–2956.
- (8) Millan, J. A.; Ortiz, D.; Glotzer, S. C. Effect of Shape on the Self-assembly of Faceted Patchy Nanoplates with Irregular Shape into Tiling Patterns. *Soft Matter* **2015**, *11*, 1386–1396.
- (9) Lohse, S. E.; Murphy, C. J. The Quest for Shape Control: A History of Gold Nanorod Synthesis. *Chem. Mater.* **2013**, 25, 1250–1261.
- (10) Habas, S. E.; Lee, H.; Radmilovic, V.; Somorjai, G. A.; Yang, P. Shaping Binary Metal Nanocrystals through Epitaxial Seeded Growth. *Nat. Mater.* **2007**, *6*, 692–697.
- (11) Xia, Y.; Gilroy, K. D.; Peng, H.-C.; Xia, X. Seed-Mediated Growth of Colloidal Metal Nanocrystals. *Angew. Chem., Int. Ed.* **2017**, *56*, 60–95.
- (12) DeSantis, C. J.; Weiner, R. G.; Radmilovic, A.; Bower, M. M.; Skrabalak, S. E. Seeding Bimetallic Nanostructures as a New Class of Plasmonic Colloids. *J. Phys. Chem. Lett.* **2013**, *4*, 3072–3082.
- (13) Buck, M. R.; Bondi, J. F.; Schaak, R. E. A Total-synthesis Framework for the Construction of High-order Colloidal Hybrid Nanoparticles. *Nat. Chem.* **2012**, *4*, 37–44.
- (14) Koczkur, K. M.; Skrabalak, S. E. *Metal Nanocrystals*; American Chemical Society: Washington DC, 2020; p 164.

- (15) Libbrecht, K. G. The Physics of Snow Crystals. Rep. Prog. Phys. 2005, 68, 855–895.
- (16) Yokoyama, E.; Kuroda, T. Pattern Formation in Growth of Snow Crystals Occurring in the Surface Kinetic Process and the Diffusion Process. *Phys. Rev. A: At., Mol., Opt. Phys.* **1990**, *41*, 2038–2049.
- (17) Weiner, R. G.; Kunz, M. R.; Skrabalak, S. E. Seeding a New Kind of Garden: Synthesis of Architecturally Defined Multimetallic Nanostructures by Seed-Mediated Co-Reduction. *Acc. Chem. Res.* **2015**, *48*, 2688–2695.
- (18) DeSantis, C. J.; Peverly, A. A.; Peters, D. G.; Skrabalak, S. E. Octopods versus Concave Nanocrystals: Control of Morphology by Manipulating the Kinetics of Seeded Growth via Co-Reduction. *Nano Lett.* 2011, 11, 2164–2168.
- (19) DeSantis, C. J.; Sue, A. C.; Bower, M. M.; Skrabalak, S. E. Seed-Mediated Co-reduction: A Versatile Route to Architecturally Controlled Bimetallic Nanostructures. *ACS Nano* **2012**, *6*, 2617–2628.
- (20) Zhang, H.; Jin, M.; Xia, Y. Noble-Metal Nanocrystals with Concave Surfaces: Synthesis and Applications. *Angew. Chem., Int. Ed.* **2012**, *51*, 7656–7673.
- (21) DeSantis, C. J.; Skrabalak, S. E. Core Values: Elucidating the Role of Seed Structure in the Synthesis of Symmetrically Branched Nanocrystals. J. Am. Chem. Soc. 2013, 135, 10–13.
- (22) Smith, J. D.; Bladt, E.; Burkhart, J. A. C.; Winckelmans, N.; Koczkur, K. M.; Ashberry, H. M.; Bals, S.; Skrabalak, S. E. Defect-Directed Growth of Symmetrically Branched Metal Nanocrystals. *Angew. Chem., Int. Ed.* **2020**, *59*, 943–950.
- (23) Patala, S.; Marks, L. D.; Olvera de la Cruz, M. Elastic Strain Energy Effects in Faceted Decahedral Nanoparticles. *J. Phys. Chem. C* **2013**, *117*, 1485–1494.
- (24) Patala, S.; Marks, L. D.; Olvera de la Cruz, M. Thermodynamic Analysis of Multiply Twinned Particles: Surface Stress Effects. *J. Phys. Chem. Lett.* **2013**, *4*, 3089–3094.
- (25) Weiner, R. G.; DeSantis, C. J.; Cardoso, M. B. T.; Skrabalak, S. E. Diffusion and Seed Shape: Intertwined Parameters in the Synthesis of Branched Metal Nanostructures. *ACS Nano* **2014**, *8*, 8625–8635.
- (26) Bower, M. M.; DeSantis, C. J.; Skrabalak, S. E. A Quantitative Analysis of Anions and pH on the Growth of Bimetallic Nanostructures. *J. Phys. Chem. C* **2014**, *118*, 18762–18770.
- (27) Chen, A. N.; Scanlan, M. M.; Skrabalak, S. E. Surface Passivation and Supersaturation: Strategies for Regioselective Deposition in Seeded Syntheses. *ACS Nano* **2017**, *11*, 12624–12631.
- (28) Weiner, R. G.; Skrabalak, S. E. Metal Dendrimers: Synthesis of Hierarchically Stellated Nanocrystals by Sequential Seed-Directed Overgrowth. *Angew. Chem., Int. Ed.* **2015**, *54*, 1181–1184.
- (29) Smith, J. D.; Scanlan, M. M.; Chen, A. N.; Ashberry, H. M.; Skrabalak, S. E. Kinetically Controlled Sequential Seeded Growth: A General Route to Crystals with Different Hierarchies. *ACS Nano* **2020**, *14*, 15953–15961.
- (30) DeSantis, C. J.; Skrabalak, S. E. Size-Controlled Synthesis of Au/Pd Octopods with High Refractive Index Sensitivity. *Langmuir* **2012**, 28, 9055–9062.
- (31) Smith, A. F.; Harvey, S. M.; Skrabalak, S. E.; Weiner, R. G. Engineering High Refractive Index Sensitivity through the Internal and External Composition of Bimetallic Nanocrystals. *Nanoscale* **2016**, *8*, 16841–16845.
- (32) Albrecht, W.; Bladt, E.; Vanrompay, H.; Smith, J. D.; Skrabalak, S. E.; Bals, S. Thermal Stability of Gold/Palladium Octopods Studied in Situ in 3D: Understanding Design Rules for Thermally Stable Metal Nanoparticles. *ACS Nano* **2019**, *13*, 6522–6530.
- (33) Quintanilla, M.; Kuttner, C.; Smith, J. D.; Seifert, A.; Skrabalak, S. E.; Liz-Marzán, L. M. Heat Generation by Branched Au/Pd Nanocrystals: Influence of Morphology and Composition. *Nanoscale* **2019**, *11*, 19561–19570.
- (34) Weiner, R. G.; Skrabalak, S. E. Seed-Mediated Co-reduction as a Route To Shape-Controlled Trimetallic Nanocrystals. *Chem. Mater.* **2016**, 28, 4139–4142.
- (35) Kunz, M. R.; McClain, S. M.; Chen, D. P.; Koczkur, K. M.; Weiner, R. G.; Skrabalak, S. E. Seed-mediated Co-reduction in a Large

- Lattice Mismatch System: Synthesis of Pd-Cu Nanostructures. *Nanoscale* **2017**, *9*, 7570–7576.
- (36) Mourdikoudis, S.; Liz-Marzán, L. M. Oleylamine in Nanoparticle Synthesis. *Chem. Mater.* **2013**, *25*, 1465–1476.
- (37) Greeley, J.; Stephens, I. E. L.; Bondarenko, A. S.; Johansson, T. P.; Hansen, H. A.; Jaramillo, T. F.; Rossmeisl, J.; Chorkendorff, I.; Nørskov, J. K. Alloys of Platinum and Early Transition Metals as Oxygen Reduction Electrocatalysts. *Nat. Chem.* **2009**, *1*, 552–556.
- (38) Gamler, J. T. L.; Leonardi, A.; Ashberry, H. M.; Daanen, N. N.; Losovyj, Y.; Unocic, R. R.; Engel, M.; Skrabalak, S. E. Achieving Highly Durable Random Alloy Nanocatalysts through Intermetallic Cores. *ACS Nano* **2019**, *13*, 4008–4017.
- (39) Gamler, J. T. L.; Ashberry, H. M.; Sang, X.; Unocic, R. R.; Skrabalak, S. E. Building Random Alloy Surfaces from Intermetallic Seeds: A General Route to Strain-Engineered Electrocatalysts with High Durability. *ACS Appl. Nano Mater.* **2019**, *2*, 4538–4546.
- (40) Wang, C.; Sang, X.; Gamler, J. T. L.; Chen, D. P.; Unocic, R. R.; Skrabalak, S. E. Facet-Dependent Deposition of Highly Strained Alloyed Shells on Intermetallic Nanoparticles for Enhanced Electrocatalysis. *Nano Lett.* **2017**, *17*, 5526–5532.
- (41) Bueno, S. L. A.; Ashberry, H. M.; Shafei, I.; Skrabalak, S. E. Building Durable Multimetallic Electrocatalysts from Intermetallic Seeds. *Acc. Chem. Res.* **2021**, *54*, 1662–1672.
- (42) Bueno, S. L. A.; Gamler, J. T. L.; Skrabalak, S. E. Ligand-Guided Growth of Alloyed Shells on Intermetallic Seeds as a Route toward Multimetallic Nanocatalysts with Shape-Control. *ChemNanoMat* **2020**, *6*, 783–789.
- (43) Yan, Y.; Du, J. S.; Gilroy, K. D.; Yang, D.; Xia, Y.; Zhang, H. Intermetallic Nanocrystals: Syntheses and Catalytic Applications. *Adv. Mater.* **2017**, *29*, 1605997.
- (44) Gamler, J. T. L.; Ashberry, H. M.; Skrabalak, S. E.; Koczkur, K. M. Random Alloyed versus Intermetallic Nanoparticles: A Comparison of Electrocatalytic Performance. *Adv. Mater.* **2018**, *30*, 1801563.
- (45) Chen, A. N.; Skrabalak, S. E. Molecular-like Selectivity Emerges in Nanocrystal Chemistry. *Dalton Trans.* **2020**, 49, 12530–12535.
- (46) Gilroy, K. D.; Peng, H.-C.; Yang, X.; Ruditskiy, A.; Xia, Y. Symmetry Breaking during Nanocrystal Growth. *Chem. Commun.* **2017**, 53, 4530–4541.
- (47) Smith, J. D.; Woessner, Z. J.; Skrabalak, S. E. Branched Plasmonic Nanoparticles with High Symmetry. *J. Phys. Chem. C* **2019**, *123*, 18113–18123.
- (48) Smith, A. F.; Weiner, R. G.; Skrabalak, S. E. Symmetry-Dependent Optical Properties of Stellated Nanocrystals. *J. Phys. Chem.* C **2016**, *120*, 20563–20571.
- (49) Zhu, C.; Zeng, J.; Tao, J.; Johnson, M. C.; Schmidt-Krey, I.; Blubaugh, L.; Zhu, Y.; Gu, Z.; Xia, Y. Kinetically Controlled Overgrowth of Ag or Au on Pd Nanocrystal Seeds: From Hybrid Dimers to Nonconcentric and Concentric Bimetallic Nanocrystals. *J. Am. Chem. Soc.* **2012**, *134*, 15822–15831.
- (50) Buck, M. R.; Schaak, R. E. Emerging Strategies for the Total Synthesis of Inorganic Nanostructures. *Angew. Chem., Int. Ed.* **2013**, *52*, 6154–6178.
- (51) Ringe, E.; McMahon, J. M.; Sohn, K.; Cobley, C.; Xia, Y.; Huang, J.; Schatz, G. C.; Marks, L. D.; Van Duyne, R. P. Unraveling the Effects of Size, Composition, and Substrate on the Localized Surface Plasmon Resonance Frequencies of Gold and Silver Nanocubes: A Systematic Single-Particle Approach. *J. Phys. Chem. C* **2010**, *114*, 12511–12516.
- (52) Kamat, P. V. Meeting the Clean Energy Demand: Nanostructure Architectures for Solar Energy Conversion. *J. Phys. Chem. C* **2007**, *111*, 2834–2860.
- (53) Jiang, R. B.; Li, B. X.; Fang, C. H.; Wang, J. F. Metal/Semiconductor Hybrid Nanostructures for Plasmon-Enhanced Applications. *Adv. Mater.* **2014**, *26*, 5274–5309.
- (54) Chen, A. N.; Endres, E. J.; Ashberry, H. M.; Bueno, S. L. A.; Chen, Y.; Skrabalak, S. E. Galvanic Replacement of Intermetallic Nanocrystals as a Route Toward Complex Heterostructures. *Nanoscale* **2021**, *13*, 2618–2625.

(55) Chen, A. N.; McClain, S. M.; House, S. D.; Yang, J. C.; Skrabalak, S. E. Mechanistic Study of Galvanic Replacement of Chemically Heterogeneous Templates. *Chem. Mater.* **2019**, *31*, 1344–1351.